J. Phys.: Condens. Matter **25** (2013) 235603 (8pp) doi:10.1088/0953-8984/25/23/235603

High temperature far-infrared dynamics of orthorhombic $NdMnO_3$: emissivity and reflectivity

Néstor E Massa[1], Leire del Campo[2,3], Domingos De Sousa Meneses[2,3], Patrick Echegut[2], María Jesús Martínez-Lope[4] and José Antonio Alonso[4]

[1] Laboratorio Nacional de Investigación y Servicios en Espectroscopía Óptica-Centro CEQUINOR, Universidad Nacional de La Plata, CC 962, 1900 La Plata, Argentina
[2] Conditions Extrêmes et Matériaux Haute Température et Irradiation (CEMHTI), 1D, Av. de la Recherche Scientifique, F-45071 Orléans, France
[3] Polytech'Orléans, Université d'Orléans, Av. du Parc Floral, BP 6749, F-45067, Orléans Cedex 2, France
[4] Instituto de Ciencia de Materiales de Madrid, CSIC, Cantoblanco, E-28049 Madrid, Spain

E-mail: neemmassa@gmail.com

Received 28 February 2013, in final form 25 April 2013
Published 16 May 2013
Online at stacks.iop.org/JPhysCM/25/235603

Abstract

We report on near normal far- and mid-infrared emission and reflectivity of $NdMnO_3$ perovskite from room temperature to sample decomposition above 1800 K. At 300 K the number of infrared active phonons is in close agreement with the 25 calculated for the orthorhombic D_{2h}^{16}–*Pbnm* ($Z = 4$) space group. Their number gradually decreases as we approach the temperature of orbital disorder at ∼1023 K where the orthorhombic O′ lower temperature cooperative phase coexists with the cubic orthorhombic O. At above ∼1200 K, the three infrared active phonons coincide with that expected for cubic *Pm*-3*m* ($Z = 1$) in the high temperature insulating regime.

Heating samples in dry air triggers double exchange conductivity by Mn^{3+} and Mn^{4+} ions and a small polaron mid-infrared band. Fits to the optical conductivity single out the octahedral antisymmetric and symmetric vibrational modes as the main phonons in the electron–phonon interactions at 875 K. For 1745 K, it is enough to consider the symmetric stretching internal mode. An overdamped defect induced Drude component is clearly outlined at the highest temperatures. We conclude that rare earth manganite e_g electrons are prone to spin, charge, orbital, and lattice couplings in an intrinsic orbital distorted perovskite lattice, favoring embryonic low energy collective excitations.

(Some figures may appear in colour only in the online journal)

1. Introduction

The families of $RMnO_3$ (R = rare earths) have been thoroughly studied over recent decades as parents of mixed valence perovskites. They have a myriad of interesting properties ranging from colossal magnetoresistance to electron ordering below a critical temperature. $NdMnO_3$, in particular, has attracted a lot of attention because it generates compounds with rich phase diagrams that may result in doping-enhanced lower dimensionalities. In these systems, electric dipoles and magnetic moments may couple, fulfilling the primary requirement for magnetoelectrics in which ferroelectricity and magnetism coexist in the so-called multiferroic phases [1].

$NdMnO_3$ is an insulator due to the absence of mixed valence states [2]. It belongs to the group of compounds with the rare earths with the largest ionic radius for which colossal magnetoresistance has been reported [3]. Nd occupies an intermediate place between La and Eu, potentially increasing the topological metastability of the

perovskite lattice as it approaches the hexagonal non-perovskite arrangement found by introducing smaller ions [2]. Its inclusion decreases the Mn–O–Mn angle, yielding a room temperature O′-orthorhombic phase belonging to the space group D_{2h}^{16}–*Pbnm* [4]. The low temperature antiferromagnetic phase of $NdMnO_3$ at $T_N \sim 78$ K is characterized by ferromagnetic alignment of the Mn moments in the ***ab*** plane. The two-fold degenerated e_g orbital breaks down and stabilizes the A-type antiferromagnetic Mn ordering [5].

At higher temperatures, between ∼1023 and ∼1273 K, two substructures, the so-called O-orthorhombic (octahedral cooperative buckling) and the O′-orthorhombic (octahedral cooperative buckling and Jahn–Teller (JT) distortion) phases coexist within a disordered orbital two-phase region [6]. Above ∼1273 K, the JT ordering distortion of MnO_6 octahedra goes undetected as it is in a net metrically cubic lattice underlying a possible dynamical JT effect [7, 8].

Below ∼973 K, the JT distortion prevails in an ordered phase that alternates a staggered pattern of $d_{3x^2-r^2}$ and $d_{3y^2-r^2}$ orbitals in the ***ab*** plane repeating itself along the ***c*** axis. The allowed Q_2 and Q_3 JT distortions compete with octahedral rotations cooperatively with marked sublattice basal plane deformations of the $GdFeO_3$-type structure [9].

Here, we report on near normal far- and mid-infrared emission and reflectivity measurements of $NdMnO_3$ from 300 K to sample decomposition. After reviewing the experimental background we introduce our high temperature data putting emphasis in the orbital disordered phase that is fundamental for understanding $NdMnO_3$ magnetoelectric couplings and phonon anharmonicities at low temperatures [10].

We have also found that heating $NdMnO_3$ in dry air activates a mid-infrared band and double exchange conductivity by Mn^{3+} and Mn^{4+} ions as in divalent A^{2+} substituted manganites [11]. This yields a scenario by which small polaron fits to the optical conductivity single out the octahedral antisymmetric and symmetric vibrational modes as main phonons in the electron–phonon interactions at 875 K. For 1745 K, it is enough to consider the symmetric stretching internal mode. We also detect above ∼1200 K an emerging overdamped defect induced Drude response characteristic of poor conducting oxides that is clearly delineated and coexists with the polaronic broad mid-infrared band [11]. At these high temperatures the number of infrared active modes coincides with that predicted for the cubic space group *Pm-3m* ($Z = 1$) (pseudocubic *Pmcm* ($Z = 1$)) [12].

2. Experimental details

Polished high quality samples in the shape of 10 mm diameter $NdMnO_3$ pellets were prepared from polycrystalline powders obtained by soft chemistry procedures.

Stoichiometric amounts of Nd_2O_3 and $MnCO_3$ were dissolved in citric acid where droplets of concentrated HNO_3 were added to favor the solution of the oxide. The citrate + nitrate solution was slowly evaporated leading to an organic resin containing a random distribution of cations. It was first dried at 120 °C and then slowly decomposed up to 600 °C. All organic material and nitrate were eliminated in a subsequent treatment for 12 h at 700 °C in air. This yielded a highly reactive precursor that was then treated at 1100 °C in a N_2-flow for 12 h. The sample was annealed in an inert atmosphere in order to avoid the formation of oxidized $NdMnO_{3-\delta}$, containing a significant amount of Mn^{4+}. $NdMnO_{3+\delta}$ was thus obtained as a well-crystallized powder. The crystal structure at ambient temperature, refined from x-ray diffraction data (figure 1), corresponds to the conventional orthorhombic space group D_{2h}^{16}–*Pbnm*. The refined unit cell parameters are $a = 5.4294(8)$, $b = 5.8438(8)$, $c = 7.574(1)$ A, in good agreement with published data [2].

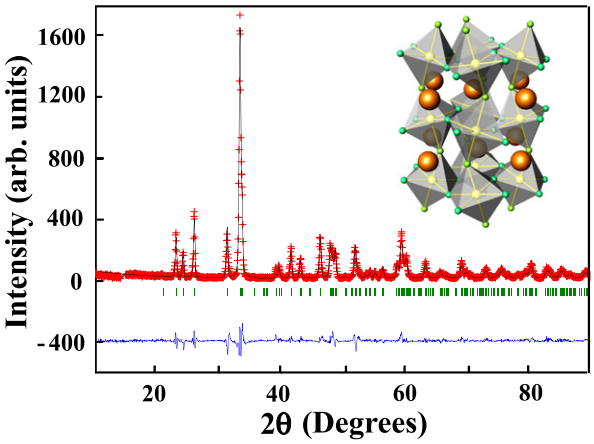

Figure 1. X-ray (Cu Kα) diffraction pattern for $NdMnO_3$. The inset corresponds to a view of the orthorhombic $NdMnO_3$ perovskite structure.

Temperature dependent medium- (MIR) and far-infrared (FIR) near normal reflectivity from 300 to 850 K was measured with a FT-IR Bruker 113v interferometer at 2 cm^{-1} resolution using a reflectance accessory. A liquid He cooled bolometer and a deuterated triglycine sulfate (DTGS) detector were employed to completely cover the spectral range of interest. A gold mirror was used as a 100% reflectivity reference since, as we show below (figure 3), 1-emissivity and reflectivity spectra are in excellent agreement. This makes possible the use of the same sample with both techniques without altering its surface (by running first reflectivity in vacuum and then emissivity in dry air). To avoid the effects of interference fringes due to the semi-transparency of $NdMnO_3$ in the THz region, we only used 2 mm or thicker samples the acceptance criteria being that they were not detected on the band profiles.

The sample and reference were placed in the sample chamber inside the spectrometer in equivalent positions related to the placement of the detector, the ratio between the sample and reference signals gave us the reflectivity spectra. For high temperature reflectivity (up to ∼850 K) we used a heating plate adapted to the near normal reflectivity attachment in the Bruker 113v vacuum chamber. In this temperature range, the spurious infrared signal introduced by the thermal radiation from the hot sample was corrected to obtain the reflectivity values. All our measurements were taken on heating runs.

Phonon normal emissivity was measured with two Fourier transform infrared spectrometers, Bruker Vertex 80v and Bruker Vertex 70, which were optically coupled to a rotating table placed inside a dry air box (see [13] for a device description and scheme). The actual experimental set up is a modification of the device thoroughly described in [14]. The use of two spectrometers allows us to simultaneously measure the spectral emittance in two dissimilar spectral ranges from 40 to 7000 cm^{-1}. The sample, which was heated with a 500 W pulse coherent CO_2 laser, was positioned on the rotating table at the focal point of both spectrometers in a position equivalent to that of internal radiation sources inside the spectrometers. In this measuring configuration, the sample, placed outside the spectrometer, is the infrared radiation source and, conversely, the sample chamber inside the spectrometers is empty (see [15]).

We will now briefly review the background of emission measurements. The normal spectral emissivity of the sample, $\boldsymbol{E}(\omega, T)$, is given by the ratio of its luminescence ($\mathscr{P}_S$) relative to the black body's luminescence ($\mathscr{P}_{BB}$) at the same temperature T and geometrical conditions, thus,

$$\boldsymbol{E}(\omega, T) = \frac{L_S(\omega, T)}{L_{BB}(\omega, T)}. \tag{1}$$

In practice, the evaluation of this quantity needs the use of a more complex expression because the measured fluxes are polluted by parasitic radiation. This is because part of the spectrometer and detectors are at 300 K. To eliminate this environmental contribution the sample emissivity is retrieved from three measured interferograms by applying the following expression [15]:

$$\boldsymbol{E}(\omega, T) = \frac{\mathrm{FT}(I_S - I_{RT})}{\mathrm{FT}(I_{BB} - I_{RT})} \times \frac{\mathscr{P}(T_{BB}) - \mathscr{P}(T_{RT})}{\mathscr{P}(T_S) - \mathscr{P}(T_{RT})} \boldsymbol{E}_{BB} \tag{2}$$

where FT stands for Fourier transform and I for measured interferograms, i.e. sample I_S; black body I_{BB}, and environment I_{RT}. $\mathscr{P}$ is Planck's function taken at different temperatures T; i.e. sample T_S, blackbody T_{BB}, and surroundings T_{RT}. $\boldsymbol{E}_{BB}$ is a correction that corresponds to the normal spectral emissivity of the black body reference (a $LaCrO_3$ Pyrox PY 8 commercial oven) and takes into account its non-ideality [15].

Emissivity allows contact free measurement of the temperature of an insulator using the Christiansen frequency, i.e. the frequency where the refractive index is equal to one and the extinction coefficient is negligible, just after the highest longitudinal optical phonon frequency. The temperature is calculated using equation (2) with the emissivity $E(\omega, T)$ at that frequency set equal to one. At higher temperatures, we have also used a thermocouple since the Christiansen inflection is absent in conducting samples.

After acquiring the optical data we placed all our spectra in a more familiar near normal reflectivity framework by noting that

$$R = 1 - E \tag{3}$$

where R is the sample reflectivity. This allows computing phonon frequencies using a standard multioscillator dielectric simulation [16]. We use a description of the dielectric function, $\varepsilon(\omega)$, given by

$$\varepsilon(\omega) = \varepsilon_1(\omega) - \mathrm{i}\varepsilon_2(\omega) = \varepsilon_\infty \prod_j \frac{(\omega_{jLO}^2 - \omega^2 + \mathrm{i}\gamma_{jLO}\omega)}{(\omega_{jTO}^2 - \omega^2 + \mathrm{i}\gamma_{jTO}\omega)} \tag{4}$$

ε_∞ is the high frequency dielectric constant taking into account electronic contributions; ω_{jTO} and ω_{jLO} are the transverse and longitudinal optical mode frequencies and γ_{jTO} and γ_{jLO} their respective damping. When needed, we also added the Drude term (plasma contribution) to the dielectric simulation as

$$-\frac{(\omega_{pl}^2 + \mathrm{i}(\gamma_{pl} - \gamma_0)\omega)}{(\omega - \mathrm{i}\gamma_0)\omega} \tag{5}$$

where ω_{pl} is the plasma frequency, γ_{pl} its damping, and γ_0 is understood as a phenomenological damping introduced to reflect lattice drag effects. When these two dampings are set equal, one retrieves the classical Drude formula [17].

The real ($\varepsilon_1(\omega)$) and imaginary ($\varepsilon_2(\omega)$) part of the dielectric function (complex permittivity, $\varepsilon^*(\omega)$) is then estimated from fitting [18] the data using the reflectivity R given by

$$R(\omega) = \left| \frac{\sqrt{\varepsilon^*}(\omega) - 1}{\sqrt{\varepsilon^*}(\omega) + 1} \right|^2. \tag{6}$$

We also calculated the real part of the temperature dependent optical conductivity, $\sigma_1(\omega)$ [19], given by

$$\sigma_1(\omega) = \frac{\omega\varepsilon_2}{4\pi}. \tag{7}$$

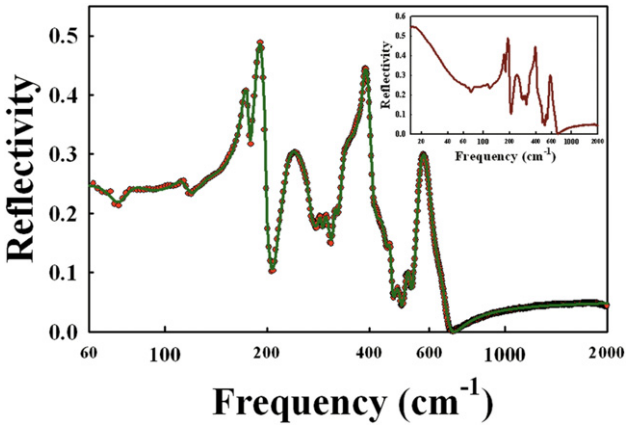

Figure 2. $NdMnO_3$ phonon near normal reflectivity at 300 K; experimental—dots, full line—fit. Inset: semilog plot of the complete far-infrared near normal reflectivity of $NdMnO_3$ at 300 K.

3. Results and discussion

Figure 2 shows the $NdMnO_3$ phonon reflectivity spectrum at room temperature. Its inset shows a smooth band originating in collective excitations active in the THz region. It locks into two concomitant soft modes at T_N that grow in intensity and

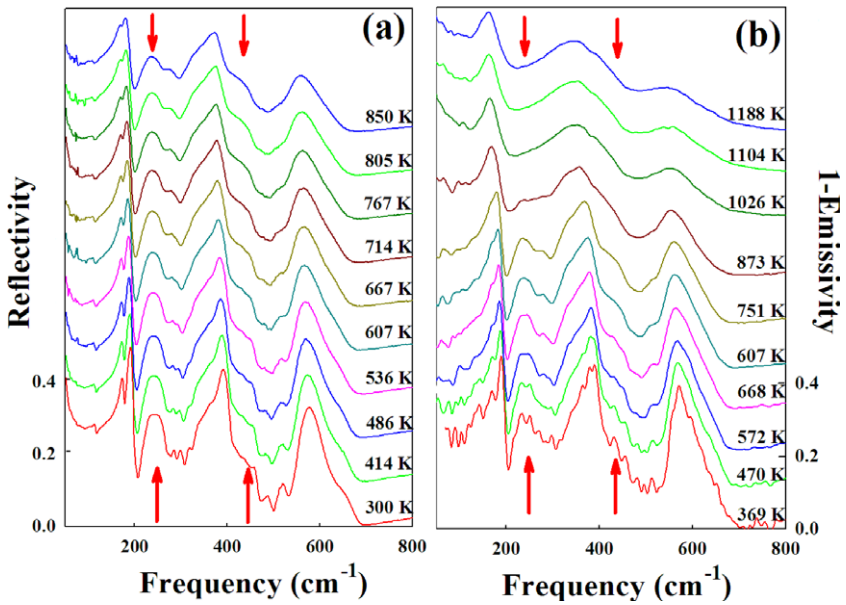

Figure 3. The same sample of $NdMnO_3$ at high temperature with (a) near normal reflectivity and (b) 1-emissivity in the vibrational region. Arrows point to vibrational groups denoting the gradual increase of orbital disorder that renders the 'O' phase net higher temperature–higher lattice symmetry above ∼1100 K. For better viewing the spectra have been displaced vertically by 0.10 relative to each other.

definition as the temperature is lowered down to 4 K [10]. Here, and although our reflectivities suggest that the 300 K smooth band persists at higher temperatures, we will not discuss this point further because of our high temperature instrumental limitation at very low frequencies.

The evolution of the near normal far-infrared emissivity and reflectivity phonon spectra of $NdMnO_3$ up to 1200 K is shown in figure 3. With increasing temperature, the reflectivity measurements obtained with the interferometer vacuum chamber are compared against those taken with the same sample heated inside the emission dry air chamber. Figure 3 displays the excellent absolute correspondence between the phonon spectra taken under near normal reflectivity and those by emission in the lower temperature range.

The reflectivity of the vacuum heated sample (figure 3(a)) shows phonon peak position softening and band broadening due to lattice anharmonicities. Phonon bands measured by emission and plotted as 1-emissivity (figure 3(b)) have the same frequency softening and band broadening up to about 800 K. Relatively weaker bands, at ∼250 and ∼450 cm^{-1}, show smooth broadening merging into the three bands found by increasing the temperature. This effect suggests that the change into an orbital disordered phase expected between 1023 K (where we find a band count already as for the three expected in the cubic phase) and 1273 K [6] takes place gradually instead of at a well-defined temperature range. The overall heating temperature dependent effects are fully reversible.

A multioscillator fit (equation (5)) to the phonon reflectivity spectrum at 300 K (figure 2), results in 24 active modes (table 1) out of the 25 predicted for the orthorhombic space group *Pbnm* ($D_{2h}^{16} - Z = 4$) [4]

$$\Gamma_{IR}(O') = 9B_{1u} + 7B_{2u} + 9B_{3u}. \quad (8)$$

At 873 K only 17 oscillators (table 1) are needed for an excellent fit, suggesting a higher temperature dynamic net increase in lattice symmetry, i.e. although at high temperatures octahedra distortion goes undetected, large thermal factors might be found for oxygens as in $LaMnO_3$, indicating the presence of an underlying dynamical JT effect [2, 7].

In addition, starting at about 500 K, the spectra obtained from samples heated in dry air (figure 4(a)) undergo changes at mid-infrared frequencies.

At 668 K a broad band centered at 2000 cm^{-1} emerges from the background. Its profile becomes less defined at ∼900 K due to the carriers' increased mobility and at higher temperatures it turns out to be almost undefined due to hopping conductivity by e_g electrons triggering an incipient insulator to metal transition due to small polaronic charge carriers. An overdamped zero frequency centered Drude–Lorentzian and its corresponding tail (figure 4(a), table 1) are now detected as in doped conducting oxides.

Known from annealing oxides in air, the freer conducting electrons are a consequence of the oxidation process $Mn^{3+} \rightarrow Mn^{4+} + 1e^-$ which is equivalent to divalent A^{2+} substitution [2]. Here, the occurrence of mixed Mn^{3+}–Mn^{4+} valence gives rise to the double exchange mechanism [20] in a higher-mobility–high-temperature small polaron-like scenario [11]. In our case, since the insertion of extra oxygen in a perovskite lattice is not possible, nonstoichiometry is generated by Nd and Mn vacancies [2].

Phonon screening by delocalized e_g electrons and stronger vibrational damping prevail in an orbital perturbed environment of coexisting O and O′ phases, the interval where orbital disorder takes place is broadened by ∼200 K due to the oxidation mechanism [8].

Above ∼1200 K the O-orthorhombic cubic phase is detected [2, 8] for which only three oscillators (table 1)

Table 1. Dielectric simulation fitting parameters for $NdMnO_3$.

T (K)	ε_∞	ω_{TO} (cm^{-1})	Γ_{TO} (cm^{-1})	ω_{LO} (cm^{-1})	Γ_{LO} (cm^{-1})
300	2.49	71.3	32.1	74.5	13.3
		76.6	15.9	78.3	41.3
		115.6	13.0	117.0	13.0
		140.0	38.0	142.5	40.4
		174.3	8.2	176.8	6.5
		187.4	12.6	189.4	121.3
		188.3	119.6	199.2	7.5
		202.5	11.1	205.5	10.6
		231.8	28.8	236.1	45.4
		256.7	75.8	274.2	20.5
		276.4	14.4	277.7	15.9
		288.5	27.4	290.9	8.8
		291.3	12.3	314.7	21.4
		312.7	77.8	315.9	24.2
		332.6	24.2	338.6	300.4
		339.8	38.3	142.5	40.4
		385.6	23.8	387.7	29.6
		396.8	49.8	406.3	26.6
		441.4	54.3	445.5	30.8
		462.3	22.1	465.6	12.8
		522.3	30.4	529.0	20.3
		556.8	30.0	559.0	53.0
		566.6	60.07	607.0	79.9
		669.2	134.0	673.5	49.7
873	1.07	49.5	424.4	58.9	173.3
		89.7	86.4	102.1	103.0
		167.0	64.4	177.2	68.0
		179.6	22.4	193.9	19.0
		236.2	55.3	256.3	52.1
		280.3	455.0	299.3	32.3
		283.5	84.0	309.5	22.7
		309.1	22.5	323.5	57.5
		315.7	56.8	387.1	39.2
		318.7	56.5	346.2	442.7
		375.6	47.6	384.7	546.5
		420.8	147.6	442.6	205.7
		449.8	103.8	460.8	73.7
		479.5	586.3	511.6	105.8
		509.8	57.8	529.2	66.1
		543.9	40.1	619.6	701.1
		616.6	197.0	639.1	95.8
		1682.9	1702.6	1904.4	6202.0
1745	1.03	155.1	61.4	183.1	68.1
		334.3	157.9	455.3	184.5
		538.1	144.3	600.5	216.0
		3603.8	6354.4	6790.7	5267.4
				ω_{pl} (cm^{-1})	
			9732.1	3658.8	10 562.7

are needed to fit our highest temperature emissivity spectra (figure 4). They are assigned to the three infrared active phonons of the reduced representation $\Gamma = 3F_{1u} + 1F_{2u}$ predicted for the high temperature cubic space group *Pm-3m* ($Z = 1$) (pseudocubic *Pmcm* ($Z = 1$)) [12].

Overall, we find that our 1-emissivity spectra show remarkable similarities with the known behavior of bulk disordered conducting oxides undergoing a metal to insulating phase transition (figure 7 in [21]). This suggests that a quantitative analysis of the high temperature mid-infrared real part of the optical conductivity, equation (7), within a small polaron context, may help to identify phonon groups involved in main carrier–phonon interactions. The coexistence of localized and itinerant carriers promoted by the strong interactions between charge carriers and ions yields the formation of polarons in highly polarizable distorted oxygen orbitals.

For this purpose, we use the theoretical formulation for small polarons due to nondiagonal phonon transitions as proposed by Reik and Heese [22, 23]. In this model, optical

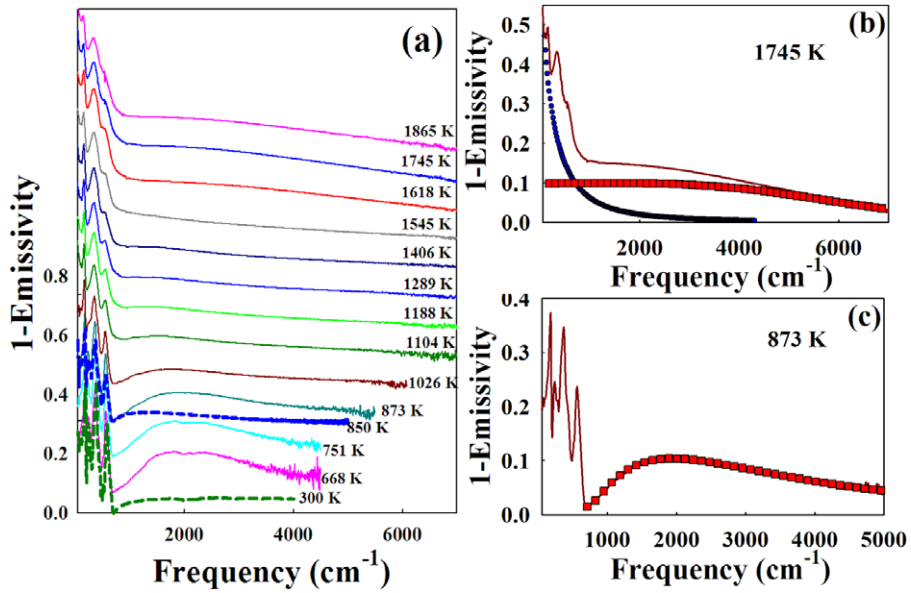

Figure 4. (a) Temperature dependent near normal 1-emissivity of $NdMnO_3$ heated in air showing the small polaron band centered at 2000 cm^{-1} and its evolution into an overdamped Drude tail at ∼1600 K. The mid-infrared spectra below 700 K have been cut because the sample is only partially absorbent. There are not enough heat-generated defects within the gap and transparency induces high levels of noise. The reflectivity of $NdMnO_3$ heated in vacuum is shown by dashed lines at 300 and 850 K. For better viewing, the spectra have been vertically shifted relative to each other by 0.10. (b) $NdMnO_3$ near normal 1-emissivity at 1745 K. The individual Drude (dots) and mid-infrared band (squares) contributions to the 1-emissivity are outlined; (c) $NdMnO_3$ near normal 1-emissivity at 873 K. The individual mid-infrared band contribution is outlined (squares).

properties are assigned to carriers in one small band and interband transitions are excluded. Starting with a Holstein's Hamiltonian [24], the frequency dependent conductivity is calculated using Kubo's formula [25]. Then, the real part of the optical conductivity for finite temperature, $\sigma_1(\omega, \beta)$ is given by

$$\sigma_1(\omega, \beta) = \sigma_{DC} \frac{\sinh(\frac{1}{2}\hbar\omega\beta)\exp[-\omega^2\Psi^2 r(w)]}{\frac{1}{2}\hbar\omega\beta[1+(\omega\Psi\Delta)^2]^{1/4}}, \tag{9}$$

$$r(\omega) = \left(\frac{2}{\omega\Psi\Delta}\right)\ln\{\omega\Psi\Delta + [1+(\omega\Psi\Delta)^2]^{1/2}\} - \left[\frac{2}{(\omega\Psi\Delta)^2}\right]\{[1+(\omega\Psi\Delta)^2]^{1/2} - 1\}, \tag{10}$$

with

$$\Delta = 2\varpi_j\Psi \tag{11}$$

and

$$\Psi^2 = \frac{[\sinh(\frac{1}{2}\hbar\varpi_j\beta)]}{2\varpi_j^2\eta}. \tag{12}$$

The conductivity, $\sigma_1(\omega, \beta)$, $\beta = 1/kT$, is mainly three-parameter dependent: the electrical DC conductivity $\sigma_{DC} = \sigma(0, \beta)$; the frequency ϖ_j that corresponds to the average between the transverse and the longitudinal optical mode of the *j*th *r*estrahlen band; and η, a parameter characterizing the strength of the electron–phonon interaction, i.e. the average number of phonons that contribute to the polarization around a localized polaron. Among all these parameters, η is the only free parameter in the optical conductivity computation

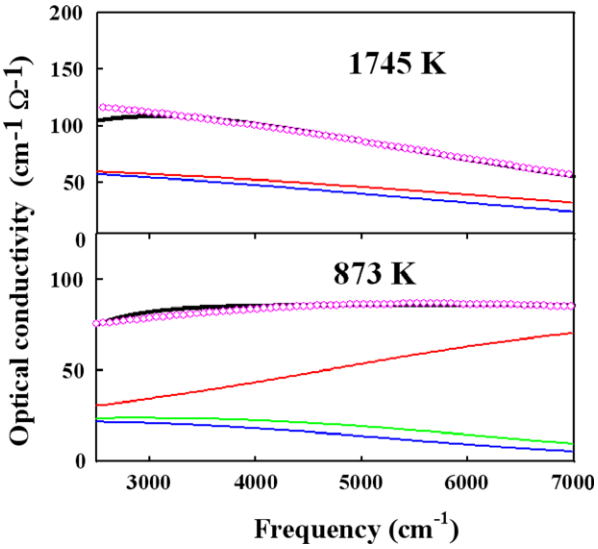

Figure 5. Temperature dependent optical conductivity of $NdMnO_3$ at 1745 and 873 K: full line—experimental; dots—fit. The fit assumes that conductivity is the sum of Gaussian-like (equation (9)) contributions (drawn in full lines), each calculated at a phonon frequency ϖ_j and at a temperature T (see text and table 2).

for each phonon frequency ϖ_j. This is because phonon frequencies are fixed by the reflectivity (or 1-emissivity) measurements and the DC-zero frequency–conductivity is known from independent, either optical or transport, measurements [26]. $\eta \sim 3$ implies a low to mild electron–phonon interaction while a value around 14 would correspond to a very strong interaction [27].

Table 2. Parameters of the small polaron theory fits to the optical conductivity of $NdMnO_3$ at 873 and 1745 K as described in the text. Note that vibrational frequencies are in agreement with experimental bands (in brackets) and that the conductivity for the highest temperatures may be described by simply considering the electron–phonon interaction associated to the octahedral breathing mode and its overtone. The DC conductivities, σ_{DC}, were kept fixed.

T (K)	σ_{DC} (Ω^{-1} cm^{-1})	η_1	ϖ_{ph1} (cm^{-1})	η_2	ϖ_{ph2} (cm^{-1})	η_3	ϖ_{ph3} (cm^{-1})
873	20.1	12.8	386.1 (375.6)	9.1	473 (480.0)[a]	16.1	615.7 (616.6)
1745	65.0			8.2	590 (570.0)	5.0	1160

[a] Average of poorly defined phonon bands found in this frequency range.

We assume that frequency dependent conductivities result from the addition of Gaussian-like (equation (9)) individual contributions, each of them calculated at a phonon frequency ϖ_j and a temperature T. The fits are shown in figure 5 (table 2). The conductivities were also constrained to positive values. They are in agreement with the experimental data. A good fit at 873 K requires only allowing the first-order internal vibrational modes of $NdMnO_3$. In spite of omitting an explicit correlation between the different contributions, the fitted frequencies are very close to the experimental ones, and for the insulator $NdMnO_3$ at 873 K the electron–phonon parameters η_j ($j = 1$–3), (table 2) are in a regime for stronger localization. These values for η and the individualization of only fundamental lattice frequencies with stronger localization are findings shared with earlier results in complex oxides [28].

In contrast, when the temperature is raised up to 1745 K, in the cubic phase, the highest frequency mode at ∼570 cm^{-1}, and its overtone at ∼1140 cm^{-1}, are singular to the fit at mid-infrared frequencies. The fundamental vibration band corresponds to the octahedral breathing symmetric stretching mode that may have the total polarization enhanced by orbital disorder [29]. The electron–phonon parameters η_j ($j = 1, 2$) (table 2) are reduced by the increased electron mobility. The detected overtone implies stronger dipole moments generated by polaronic coupling between the charge and the vibrating lattice [11].

The behavior at high temperature is also coincident with earlier conclusions from thermal expansion measurements of nonstoichiometric $NdMnO_{3+\delta}$ showing large irreversible lattice anomalies on heating and cooling in the ∼1100 K temperature range [4].

We conclude from our high temperature measurements of $NdMnO_3$ that one may expect, for rare earth manganites, e_g electrons prone to strong spin–phonon couplings in an intrinsic orbital distorted perovskite lattice, favoring embryonic low energy collective excitations at all temperatures.

4. Conclusions

Summarizing, we presented temperature dependent near normal far-infrared emissivity and reflectivity spectra of $NdMnO_3$ from 300 to 1800 K. We found that when heated in air, as is known for divalent doping in manganites, oxygen excess triggers hopping conductivity within the double exchange mechanism framework. In close agreement with the expected number of 25 room temperature phonons for the space group *Pbnm* (D_{2h}^{16} $-$ $Z = 4$), the number of bands is reduced gradually up to 1200 K where there only remain three infrared active phonons associated with those allowed for cubic high temperature insulating phase space group *Pm-3m* ($Z = 1$).

Overall, our measurements give a comprehensive view of the evolution of e_g electrons at high temperatures in $NdMnO_3$ entangled d-orbitals. The environment used in the emissivity measurements allows us to infer the origin of electronic induced mechanisms for colossal magnetoresistance or polar ordering in transition metal oxides involving orbital/charge and/or spin fluctuations [30–32].

Acknowledgments

NEM is grateful to the CNRS-CEMHTI Laboratory and staff in Orléans, France, for research and financial support in performing far-infrared measurements. NEM also acknowledges partial financial support (PIP 0010) from the Argentinean Research Council (Consejo Nacional de Investigaciones Científicas y Técnicas-CONICET). Funding through Spain Ministry of Science and Innovation (Ministerio de Ciencia e Innovación) under Project MAT2010 No. 16404 is acknowledged by JAA and MJM-L.

References

[1] Wang K F, Liu J-M and Ren Z F 2009 *Adv. Phys.* **58** 321
[2] Alonso J A, Martinez-Lope M J, Casais M T and Fernández-Díaz M T 2000 *Inorg. Chem.* **39** 917
[3] Jin S, Tiefel T H, McCormack M, Fastnacht R A, Mamesh R and Chen L H 1994 *Science* **264** 413
[4] Kasper N V and Troyanchuk I O 1996 *J. Phys. Chem. Solids* **57** 1601
[5] Jandl S, Nekvasil V, Diviš M, Mukhin A A, Hölsä J and Sadowski M-L 2005 *Phys. Rev.* B **71** 024417
[6] Goodenough J B 1971 *Prog. Solid State Chem.* **5** 145
[7] Rodriguez-Carvajal J, Hennion M, Moussa F, Moudden A H, Pinsard L and Revcolevschi A 1998 *Phys. Rev.* B **57** R3189
[8] Maris G A 2004 *PhD Dissertation* Rijkuniversiteit Groningen Also Maris G, Volotchaev V and Palstra T T M 2004 *New J. Phys.* **6** 153
[9] Madelung O, Rossler U and Schultz M (ed) 2011 $GdFeO_3$ crystal structure, physical properties, *Springer Materials, The Landolt–Börnstein Database* (www.springermaterials.com)

[10] Massa N E, del Campo L, De Sousa Meneses D, Echegut P, Martínez-Lope M J and Alonso J A 2013 in preparation
[11] Calvani P 2001 Optical properties of polarons *Riv. Nuovo Chimento* **24** 1
[12] Kamba S, Nuzhnyy D, Savinov M, Šebek J, Petzelt J, Prokleška J, Haumont R and Kreisel J 2007 *Phys. Rev.* B **75** 024403
[13] del Campo L, De Souza Meneses D, Blin A, Rousseau B, Véron E, Balat-Pichelin M and Echegut P 2011 *J. Am. Ceram. Soc.* **94** 1859
[14] Rosenbaum O, De Souza Meneses D, Auger Y, Chermanne S and Echegut P 1999 *Rev. Sci. Instrum.* **70** 4020
[15] De Souza Meneses D, Brun J-F, Rousseau B and Echegut P 2006 *J. Phys.: Condens. Matter* **18** 5669
[16] Kurosawa T 1961 *J. Phys. Soc. Japan* **16** 1298
[17] Gervais F, Servoin J L, Baratoff A, Bednorz J B and Binnig G 1993 *Phys. Rev.* **47** 8187
[18] Focus Software Website, www.cemhti.cnrs-orleans.fr/pot/software/focus.html
[19] Wooten F 1972 *Optical Properties of Solids* (New York: Academic)
[20] Zener C 1951 *Phys. Rev.* **82** 403
[21] Massa N E, Dernadim J C, Socolovsky L-M, Knobel M and Zhang X X 2009 *J. Appl. Phys.* **105** 114306
[22] Reik H G 1972 *Polarons in Ionic Crystals and Polar Semiconductors* ed J T Devreese (Amsterdam: North-Holland) p 679
[23] Reik H G and Heese D 1967 *J. Phys. Chem. Solids* **28** 581
[24] Holstein T 1959 *Ann. Phys.* **8** 343
[25] Kubo R 1957 *J. Phys. Soc. Japan* **12** 570
[26] Mühlstroh R and Reik H G 1967 *Phys. Rev.* **162** 703
[27] Reik H G 1967 *Z. Phys.* **203** 346
[28] Massa N E, Denardin J C, Socolovsky L M, Knobel M, De la Cruz F P and Zhang X 2007 *Solid State Commun.* **141** 551
[29] Massa N E, Falcon H, Salva H and Carbonio R E 1997 *Phys. Rev.* B **56** 10178
[30] Keimer B 2006 *Nature Mater.* **5** 933
[31] Tokura Y and Nogaosa N 2000 *Science* **288** 462
[32] Keimer B and Oles A M 2004 *New J. Phys.* **6** E05 and references therein